Effect of milling atmosphere on structural and magnetic properties of Ni–Zn ferrite nanocrystalline*

Abdollah Hajalilou[a)†], Mansor Hashim[a)], Reza Ebrahimi-Kahrizsangi[b)], and Mohamad Taghi Masoudi[b)]

[a)] *Material Synthesis and Characterization Laboratory, Institute of Advanced Technology (ITMA), Universiti Putra Malaysia, 43400 UPM, Serdang, Selangor, Malaysia*

[b)] *Advanced Materials Research Center, Materials Engineering Department, Najafabad Branch, Islamic Azad University, Najafabad, Isfahan, Iran*

(Received 30 September 2014; revised manuscript received 8 November 2014; published online 10 February 2015)

Powder mixtures of Zn, NiO, and Fe_2O_3 are mechanically alloyed by high energy ball milling to produce Ni–Zn ferrite with a nominal composition of $Ni_{0.36}Zn_{0.64}Fe_2O_4$. The effects of milling atmospheres (argon, air, and oxygen), milling time (from 0 to 30 h) and heat treatment are studied. The products are characterized using x-ray diffractometry, field emission scanning electron microscopy equipped with energy-dispersive x-ray spectroscopy, and transmitted electron microscopy. The results indicate that the desired ferrite is not produced during the milling in the samples milled under either air or oxygen atmospheres. In those samples milled under argon, however, Zn/NiO/Fe_2O_3 reacts with a solid-state diffusion mode to produce Ni–Zn ferrite nanocrystalline in a size of 8 nm after 30-h-milling. The average crystallite sizes decrease to 9 nm and 10 nm in 30-h-milling samples under air and oxygen atmospheres, respectively. Annealing the 30-h-milling samples at 600 °C for 2 h leads to the formation of a single phase of Ni–Zn ferrite, an increase of crystallite size, and a reduction of internal lattice strain. Finally, the effects of the milling atmosphere and heating temperature on the magnetic properties of the 30-h-milling samples are investigated.

Keywords: Ni–Zn ferrite nanocrystalline, mechanical alloying, milling atmosphere, milling time, magnetic property

PACS: 81.20.Ev, 81.40.Rs, 91.60.Pn, 92.70.Cp **DOI:** 10.1088/1674-1056/24/4/048102

1. Introduction

Ni–Zn ferrites have been broadly used in electrical industries because of their special characteristics such as low eddy current loss and high permeability. The cubic spinel Ni–Zn ferrite is one of the MFe_2O_4 phase family with a face-centered $Fd\bar{3}m$ structure. A general formula for this ferrite could be written as $[Fe_{1-x}{}^{2+}Zn_x{}^{2+}]^A\ [Ni_{1-x}{}^{2+}Fe_{1+x}{}^{3+}]^BO_4$, where x denotes the degree of inversion, and B and A represent the octahedral and tetrahedral sites, respectively. Nickel ions exist at B-sites while zinc ions have a preference for A-sites, and iron ions, which depend on Zn concentration, are distributed between A and B sites. Generally speaking, two main routes are being used to synthesize these spinel ferrites: wet chemical methods, such as sol–gel, coprecipitation,[1–3] and solid-state routes such as conventional sintering at high temperatures.[4] Each of these techniques has its own advantages and disadvantages. For example, the wet chemical methods make it possible to produce very small particles at lower sintering temperatures; however, these methods are not environmentally friendly. On the other hand, a high sintering temperature is required in solid-state methods, which make them uneconomical due to the highly expensive furnaces required.

Mechanical alloying is a good replacement for the solid-state method with the additional advantages of reduced milling time and practicality which can be exploited for the speedy preparation of nanocomposites, advanced ceramics, amorphous alloys, metastables, and other important powders in large tonnages.[5–7] Furthermore, optimizing the variable parameters of the mill such as milling time, rotation speed, and ball-to-powder weight ratio can reduce cost and time.[8] A number of researches, including, but not restricted to, Refs. [9]–[12], have exploited this technique to produce the Ni–Zn ferrite nanocrystalline. They investigated the effects of certain milling parameters such as milling time, but no study has been reported yet on the effect of milling atmosphere on the products for the Ni–Zn ferrite system. The present study is to produce $Ni_{0.36}Zn_{0.64}Fe_2O_4$ nanocrysatlline by using the high energy milling process and to investigate the effects of milling time and milling atmosphere on the final product and its magnetic properties.

2. Method

Zn, NiO, and Fe_2O_3 powders were purchased from Alfa Aaser and directly used without further purification. The powders were weighed and mixed in molar ratios based on the following reaction:

$$0.36NiO + 0.64Zn + Fe_2O_3 = Ni_{0.36}Zn_{0.64}Fe_2O_4. \quad (1)$$

A ball to powder ratio was chosen to be 10:1. Then, a high energy planetary ball milling machine was run at room tempera-

*Project supported by the University Putra Malaysia Graduate Research Fellowship Section.

†Corresponding author. E-mail: e.hajalilou@yahoo.com

© 2015 Chinese Physical Society and IOP Publishing Ltd

ture under air, argon, and oxygen atmospheres. Mechanical alloying was carried out using four hardened steel vials (150 ml) accompanied by five hardened steel balls, each 18 mm in diameter. Finally, the rotational speeds of the vial and the disc were fixed at 600 rpm and 400 rpm, respectively, and the powders were activated for different periods ranging from 0 to 30 h. It is worth mentioning that the milling machine is adjusted in such a way that it has a 15-min rest after each one hour milling. This was to prevent the powder from agglomerating. After the ball milling process, 30 h-milled samples were selected to anneal at 600 °C temperatures for 2 h.

Phase and structural evaluation were studied using an x-ray diffraction (XRD) spectrometer in a diffraction angular range of $2\theta = 20°$–$80°$ and using Cu Kα (wave length $(\lambda) =$ 0.154 nm). Field emission scanning electron microscopy (FE-SEM) using a JEOL JSM-7600F machine was employed to evaluate the powder particle morphology and microstructure. Transmission electron microscopy (TEM) analyses of the samples were carried out using a Hitachi 7100 TEM (Tokyo, Japan) at 75 kV. Brunauer, Emmett, and Teller (BET) were used to measure the particle size. The vibrating sample magnetometer (VSM) was used to study the magnetic properties of the samples at room temperature. The *B*–*H* hysteresis loops of the bulk samples were studied using a MATS-2010SD Static Hysteresisgraph.

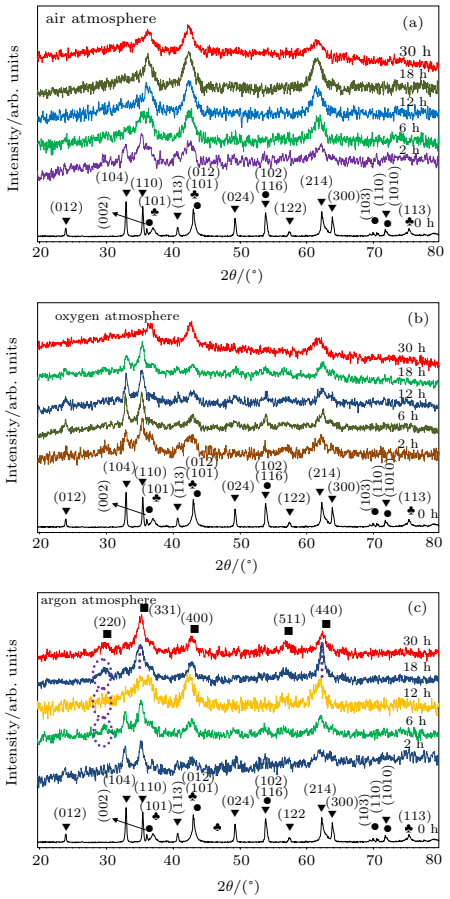


Fig. 1. (color online) The x-ray diffraction patterns of the NiO/Zn/Fe_2O_3 powder mixture after different milling times under (a) air, (b) oxygen, and (c) argon atmospheres.

3. Results and discussion

3.1. Phase and structural evaluation

The x-ray diffraction patterns of the as-received and ball-milled powder of $Ni_{0.36}Zn_{0.64}Fe_2O_4$ nanoparticles prepared under different atmospheres are shown in Fig. 1. The diffraction patterns of the starting raw materials indicate the presence of signature peaks of the three initial raw materials (i.e., Zn at $2\theta = 36.29$ ($I = 39.6$), 39.04 ($I = 23.3$), 43.22 ($I = 100$), 54.1, 70.09; NiO at $2\theta = 37.28$ ($I = 60$), 43.22 ($I = 100$), 62.85 ($I = 30$), 75.54; Fe_2O_3 at $2\theta = 24.19$, 33.18 ($I = 100$), 35.69 ($I = 71$), 40.90, 49.52, 54.1 ($I = 42$), 57.61, 62.45, 64.03, 71.95, 75.54), which can be matched with ICDD PDF#01-087-0713, ICDD PDF#04-0833, and ICDD PDF#01-1053 for Zn, NiO, and Fe_2O_3, respectively.

In the case of the powder milled under air, all the peaks of the starting materials, except for those of zinc, appear after the milling time has increased to 2 h. The disappearance of Zn peaks may be attributed to the fact that one of the three following conditions happens: 1) Zn evaporating and escaping from the system due to its low boiling point, 2) Zn becoming amorphous, and 3) Zn converting into other phases. The occurrence of ZnO peaks in the XRD pattern indicates that Zn reacts with the ambient oxygen and converts into the ZnO phase. By increasing milling time to 6 h, the peaks in the ranges $2\theta = 35°$–$36°$ and $61°$–$64°$ interfere with each other. Furthermore, slight changes are observed at the positions of the diffraction angles of the peaks. This may be attributed to the solid-solution formation. Three broad peaks are observed around $2\theta = 35°$, $41°$, and $62°$ after the milling time has been extended to 12 h; this might be due to either the formation of the (Zn, Fe)O solid-solution or the presence of Fe_2O_3, since the most intense peak of Fe_2O_3 at $2\theta = 33°$ disappears with increasing the milling duration. Furthermore, all the small peaks at other Bragg diffraction angle positions also diminished. This indicates that the peaks are due to the solid-solution formation. The results are consistent with those obtained by Bid and Pradhan,[12] which indicates that the formation of $ZnFe_2O_4$ can take place within only 30 min of ball milling with homogeneous stoichiometric (1:1 mole%) powder mixture of Fe_2O_3 and ZnO phases. When the milling time goes up to 18 h, the peaks move to the same Bragg diffraction position of Ni–Zn ferrite. This suggests the likely formation of the ferrite. As the most intense peak of Ni–Zn ferrite is located at $2\theta = 35°$, a comparison of intensity among the three peaks reveals that the peak at $2\theta = 35°$ has the lowest intensity. Furthermore, the small peak of Ni–Zn ferrite in the XRD pattern is also absent at $2\theta = 30°$. Thus, it may be concluded that those peaks cannot be attributed to the Ni–Zn ferrite, rather, they correspond to the (Ni, Zn)FeO solid-solution formation. By increasing the milling time to 30 h, no new phases are observed, but the peaks

decrease in intensity and their widths become broadened. The same trend is somewhat observed in the phase formation of the samples milled under oxygen.

In the powder milled under argon, Ni–Zn ferrite seems to be produced when the milling time reaches 2 h. This is due to the emergence of a new peak at $2\theta = 30^\circ$, which might be related to one of the ferrite diffraction peaks. On the other hand, the presence of Fe_2O_3 at $2\theta = 24^\circ$ leads to the conclusion that the peak appearing at $2\theta = 30^\circ$ cannot be associated with Ni–Zn ferrite. By indexing the Bragg diffraction angle from the JCPDS file (ICDD PDF#98-006-8765), it is clear that the peak in question is related to the Fe_3O_4 phase. In fact, this line of argument is based on the overlapping of the ferrite and iron oxide peaks. When the milling time is increased to 6 h, all the peaks of the Fe_2O_3 phase almost disappear. This can be explained by the fact that the most intense peak of Fe_2O_3 at $2\theta = 34^\circ$ also vanishes. Furthermore, the peak at $2\theta = 36^\circ$ becomes more intense and shifts to a lower diffraction angle as well. This can be due to the diffusion of NiO or ZnO in the lattice structure of iron oxides, which causes a change in its lattice parameters. Fe_2O_3 peaks emerge in the XRD pattern when the milling time is increased to 12 h. Furthermore, a slight reduction is observed in the intensity of the peaks of the Fe_3O_4 phase. This indicates that besides the formation of the solid-solution phase, Fe_2O_3 and Fe_3O_4 converted to each other during the 12 h of milling. By extending the milling time to 18 h, no more peaks pertaining to iron oxides are observed in the XRD patterns but new peaks appear at the diffraction positions of Ni–Zn ferrite. Given the fact that the peak at $2\theta = 30^\circ$ is still not available and that the peaks in a range of 2θ from 35° to 36° interfered with each other, it may be concluded that the Ni–Zn ferrite might be produced but that the reaction is not yet complete. This may be due to the fact that the NiO compounds diffuse in the lattice structure of iron oxides or $ZnFe_2O_4$ and thus form the solid-solution. It has been reported that the diffusion of zinc in the lattice structure of iron oxides is faster than that of Ni.[12] Extending the milling time to 30 h leads to the completion of the solid-solution stages and the occurrence of a new peak at $2\theta = 30^\circ$. Given the overlapping of Ni–Zn ferrite and Fe_3O_4 at this position of the diffraction angle, it may be claimed that this peak is related to either Fe_3O_4 or Ni–Zn ferrite. It can be seen that the diffraction peak at $2\theta = 63^\circ$ is less intense than at $2\theta = 36^\circ$. Therefore, it cannot be attributed to Fe_3O_4. Eventually, the Ni–Zn ferrite single phase is formed after 30 h of milling. This can be judged on the basis of the occurrence of small peaks at $2\theta = 30^\circ$ and the existence of a high intensity peak at $2\theta = 35^\circ$ as the major peak of the Ni–Zn ferrite. Furthermore, all the peaks appear following the Ni–Zn ferrite's Bragg diffraction angles according to the JCPDS file (ICDD PDF#98-006-8765). To further study the effect of the milling atmosphere on the powders milled over the same durations, FESEM and TEM images corresponding to the 30-h-milling powders under air, argon, and oxygen are taken.

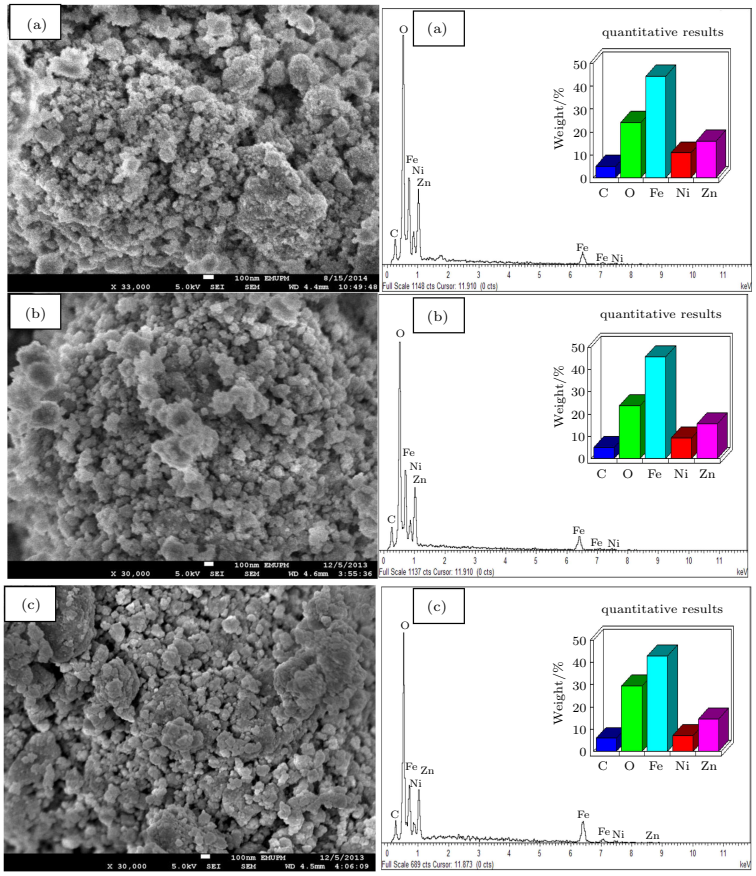


Fig. 2. (color online) FESEM images and EDX spectra of the 30-h-milling samples under (a) air, (b) argon, and (c) oxygen.

Figure 2 displays the FESEM images of the 30-h-milling samples under different atmospheres, accompanied by their corresponding EDX spectra. The FESEM images show that very fine particles are produced by the collisions of powder–ball–vial with each other. On the other hand, a rise in temperature inside the vial leads to stuck powder particles and to agglomeration. The presence of peaks pertaining to Fe, Ni, Zn, and O in the EDX spectra indicates that any impurities are introduced into the samples during the preparation and milling processes. The C peaks detected in the spectrum are because of the carbon tape used on the Al stub.

Figure 3 displays the TEM micrographs of the samples milled for 30 h under air, argon, and oxygen. The specific surface area for the powders milled for 30 h under argon is found to be 105.86 m^2/g so that the particle size ranges from 5 nm to 19 nm with a mean size of 13 nm. For the powder milled under oxygen, the specific surface area is 91.02 m^2/g, whose particle size is in a range of 7 nm–24 nm with a mean value of 16 nm. In the case of the powder milled under air, the particle distribution becomes slightly smaller and ranges from 5 nm to 21 nm with a specific surface area of 95.69 m^2/g and an average size of 15 nm. In fact, a value of x-ray density is computed based on the equation suggested by Smit and Wijn[13] as follows:

$$\rho_{\mathrm{xrd}} = 8M/N_{\mathrm{a}}a^3, \tag{2}$$

where a is the lattice constant, N_{a} is the Avogadro's number (6.02×10^{23}), and M is the molecular weight of the sample. The porosity of the sample is computed based on the following equation

$$P = [1 - (\rho_{\mathrm{exp}}/\rho_{\mathrm{xrd}})] \times 100\%, \tag{3}$$

where ρ_{xrd} is the x-ray density and ρ_{exp} is the experimental density, which is obtained from the Archimedes principle. It is found that the values of experimental density for 30 h-milling samples under air, argon, and oxygen atmospheres to be 4.18, 4.36, and 4.12 g/cm^{-3}, respectively. The specific surface area of particles is estimated by using Eq. (3) to be[14]

$$S = \frac{6000}{\rho D}, \tag{4}$$

where ρ is the experimental density and D is the average particle size.

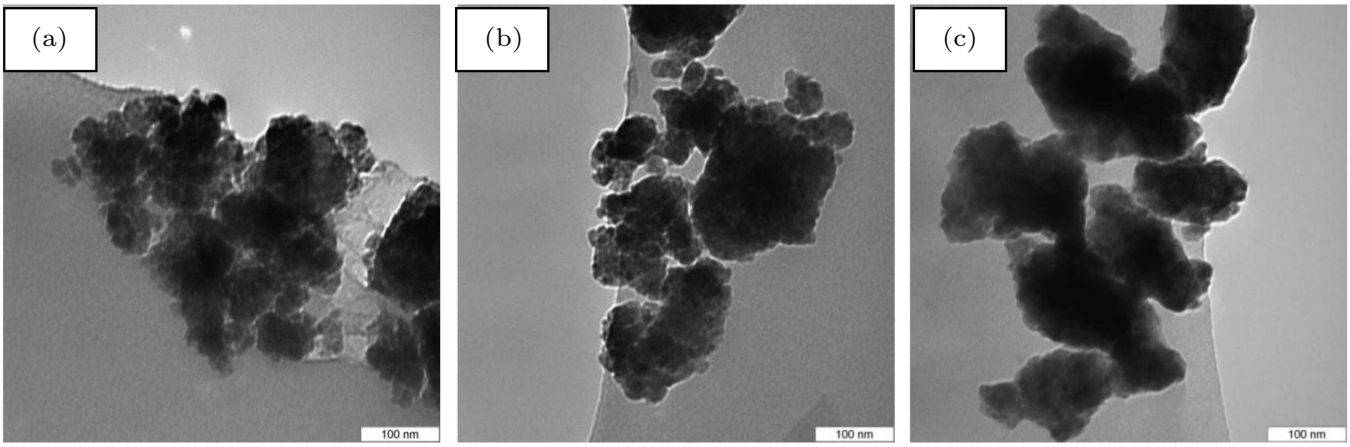


Fig. 3. TEM micrographs of the 30-h-milling samples under (a) air, (b) argon, and (c) oxygen.

3.2. Effects of milling time on the crystallite size and lattice strain

As is well known, the powder particles become frequently flattened, cold welded, fractured, and rewelded in the milling process. In fact, the characteristics of the powder deformation onset determine the occurrence of fracturing and cold welding processes, their kinetics and predominance at any step of milling. In the early milling steps, ductile metals are prone to flattening and work hardening due to the influence of the grinding medium. The particle surface-to-volume ratio increases as a result of sever plastic deformation, which ruptures the absorbed contaminants of the surface film. The brittle material then fractures and becomes smaller in size.[5] By increasing the milling duration under all the three atmospheres, the widths of the peaks are broadened and their intensities are reduced. This is due to the fact that their crystallite sizes become smaller and the internal lattice strains increase. In fact, the ball/powder/vial collisions reduce the particle sizes in the milling process. On the other hand, the creation of a large number of lattice defects such as grain boundaries and dislocations enhances the lattice strain.

The induced modifications in the size of crystallite and lattice strain of the samples are evaluated by the x-ray diffrac-

tion peak broadening, and using the following Williamson–Hall equation[15] and the X'Pert HighScore software:

$$b\cos\theta = \frac{K\lambda}{d} + 2A\sqrt{\varepsilon^2}\sin\theta, \tag{5}$$

where d, η, λ, b, and θ are the average crystallite size (nm), internal lattice strain (%), wavelength (0.145 nm), the diffraction peak width at half-maximum intensity, and Bragg's diffraction angle (rad); A is a coefficient which relies on the strain distribution; K is the Scherrer constant (usually taken to be 0.91). Their results are listed in Table 1. In fact, by ploting $b\cos\theta$ against $2\sin\theta$ as shown for the 30-h-milling sample in argon in Fig. 4, a lattice strain can be obtained from the slope of the straight line, and the y-intercept yields $0.9\lambda/d$ in which the d is the average crystallite size. It is worth mentioning that the details of this procedure were reported in our previous work.[6]

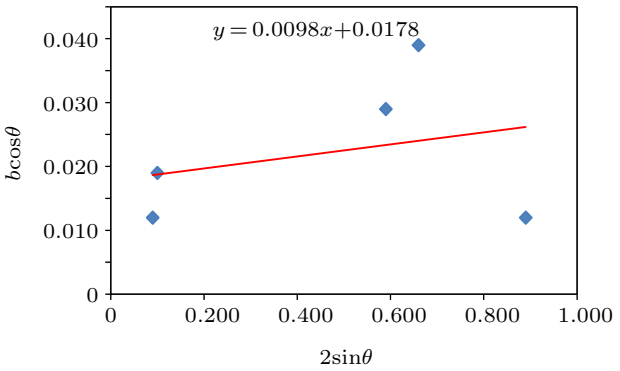


Fig. 4. (color online) Williamson–Hall equation calculation for 30-h-milling sample in argon atmosphere.

As indicated in Table 1, lattice strains continuously increase in the powder ball-milled under air and argon with increasing the milling time so that their values rise from 0.520% and 0.612% to 1.036% and 0.998%, respectively, with milling time increasing from 2 h to 30 h. The lattice strain in the powder milled under oxygen increases from 0.556% to 1.291% for milling duration between 2 h and 18 h, but decreases to 0.844% when the milling time is extended to 30 h. The reason for this increment in lattice strain is the enhancement of lattice defects and the piling up of dislocations. Whereas the reduction in its value can be associated with the dominance of the recovery rate relative to the work hardening rate.[6] A comparison of the crystallite sizes in the powders milled under the three atmospheres reveals that the powder milled under argon has the smallest crystallite size whereas those milled under the other two atmospheres have crystallite sizes approximately close to each other, in which the one milled under air has a smaller size. As can be seen in Table 1, the crystallite sizes of the powders milled under air and oxygen decrease steadily and drop to 9 nm and 10 nm, respectively, after 30 h of milling. The crystallite size in the powder milled under argon, however, decreases to 7 nm after 18 h of milling before it rises to 8 nm after 30 h of milling. The increase in the crystallite size of the powder milled from 18 h to 30 h under argon may be related to the formation of Ni–Zn ferrite and the heat released from the completion of the reaction. In fact, two actions take place simultaneously in the ball milling process: i) refinement of powder particles due to the ball–powder collisions and the associated work hardening, and ii) the increase in temperature inside the vial due to long milling durations and the completion of the reaction. These traits, therefore, cause fine particles to stick together and agglomerate.

Table 1. The values of average crystallite size (d) and lattice strain (ε) for samples milled under different atmospheres.

Milling time/h	Oxygen atmosphere		Argon atmosphere		Air atmosphere	
	d/nm	ε/%	d/nm	ε/%	d/nm	ε/%
2	17	0.556	14	0.612	15	0.581
6	15	0.652	10	0.726	13	0.601
12	13	0.735	11	0.874	14	0.693
18	12	1.291	7	0.927	11	0.942
30	10	0.844	8	0.988	9	1.036

3.3. Evaluation of morphological changes in ball-milled samples

The milled powder under argon atmosphere, for example, is selected to further study the effect of milling time on the powder particle by FESEM analysis. Figure 5 shows the FESEM images of ball-milled powder morphology after different milling times. It should be mentioned that all the images are taken at the same magnification of 3×10^4 and on a scale of 100 nm. As can be observed, after the simple mixing of powders (0 h), the powder morphology exhibits an approximately spherical shape with an inhomogeneous distribution. This is due to the fact that no reaction takes place between the reactants only after simple mixing. By increasing the milling time to 2 h, new phases burgeon, the sizes of the particles decrease, and the homogeneous distribution increases gradually. After 6 h of milling, the powder particles frequently fragment and are cold welded together. In fact, work hardening of the powder occurs and fracturing overcomes the cold welding, resulting in a much finer particle size and a more homogeneous distribution. By increasing the milling time to 12 h and 18 h, no significant changes are observed in the morphologies of the powder. This can be associated with the equal rates of fracturing and cold welding. By elevating the milling time to 30 h, the powder particles stick to each other and agglomerate. This indicates that for higher milling times, cold welding overcomes fracturing. In fact, by increasing the milling time, the powder particles become smaller and heat is released from the reactants. Thus the increased temperature inside the vial leads to the agglomeration of powder particles.

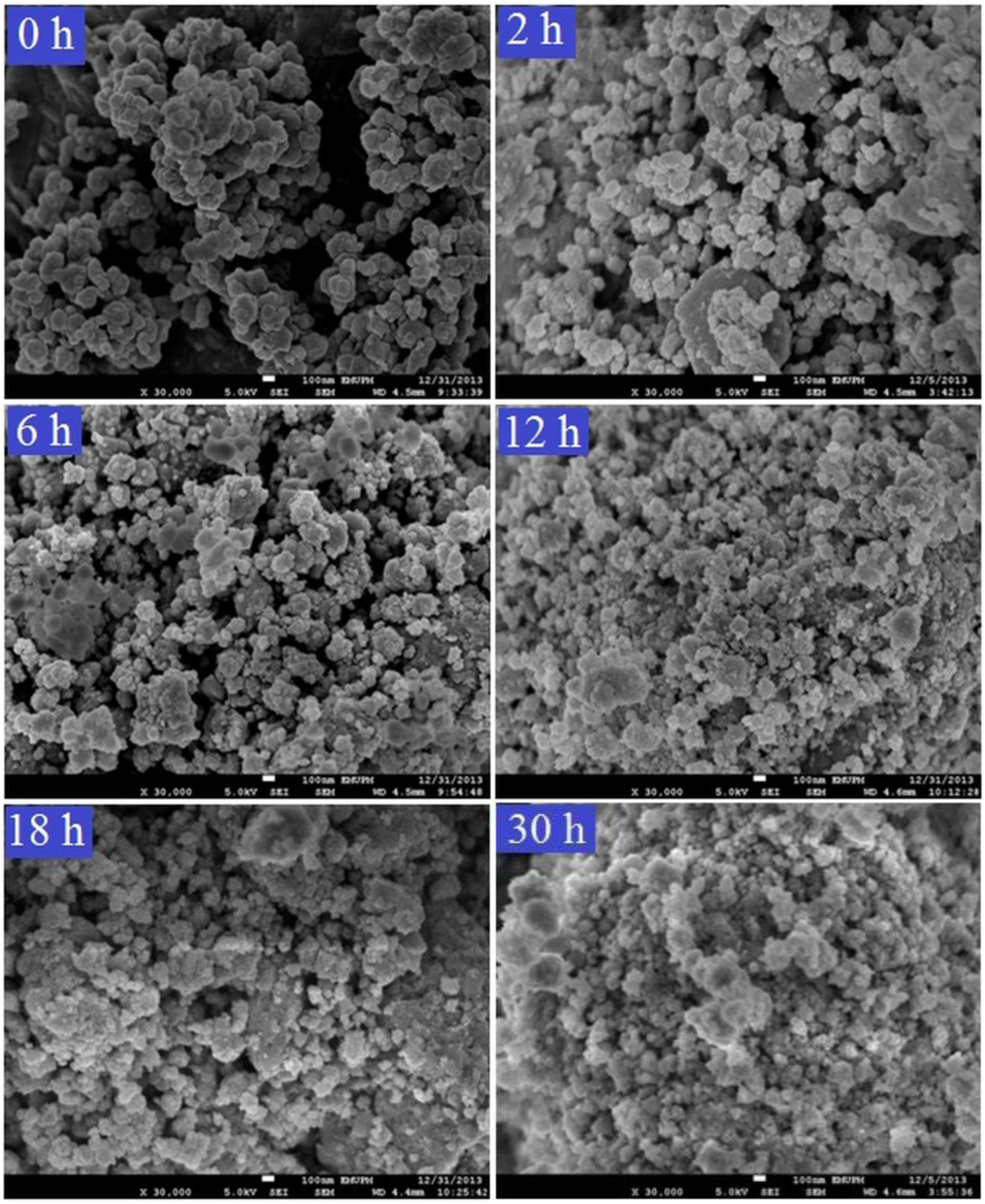


Fig. 5. FESEM images of the powder particles after different milling times.

3.4. Annealing process

The particle size, distribution, crystallization, and shape of polycrystalline material are affected by the heating process, which results in the attainment of the right metal proportion at a proper valence, hence, thereby improving the desirable properties.[16] To study the decisive role played by annealing in the microstructure, the mean crystallite size, lattice strain evolution, and phase formation, the 30-h-milling powder under argon, oxygen, and air atmospheres are heated at 600 °C. Figure 6 displays the XRD patterns of the 30-h-milling samples under different atmospheres subjected to heat treatment at a temperature of 600 °C.

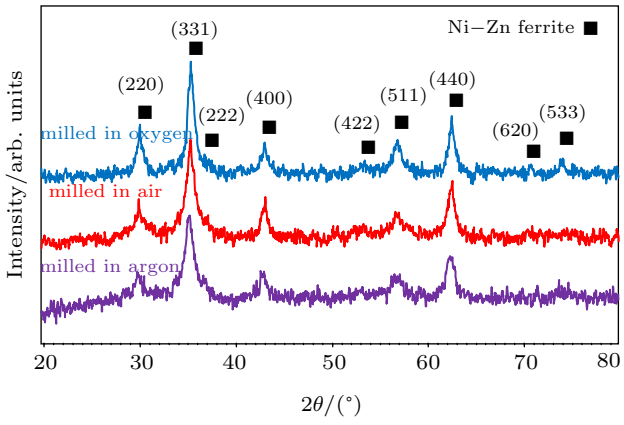


Fig. 6. (color online) XRD patterns of the 30-h-milling samples under different atmospheres sintered at 600 °C.

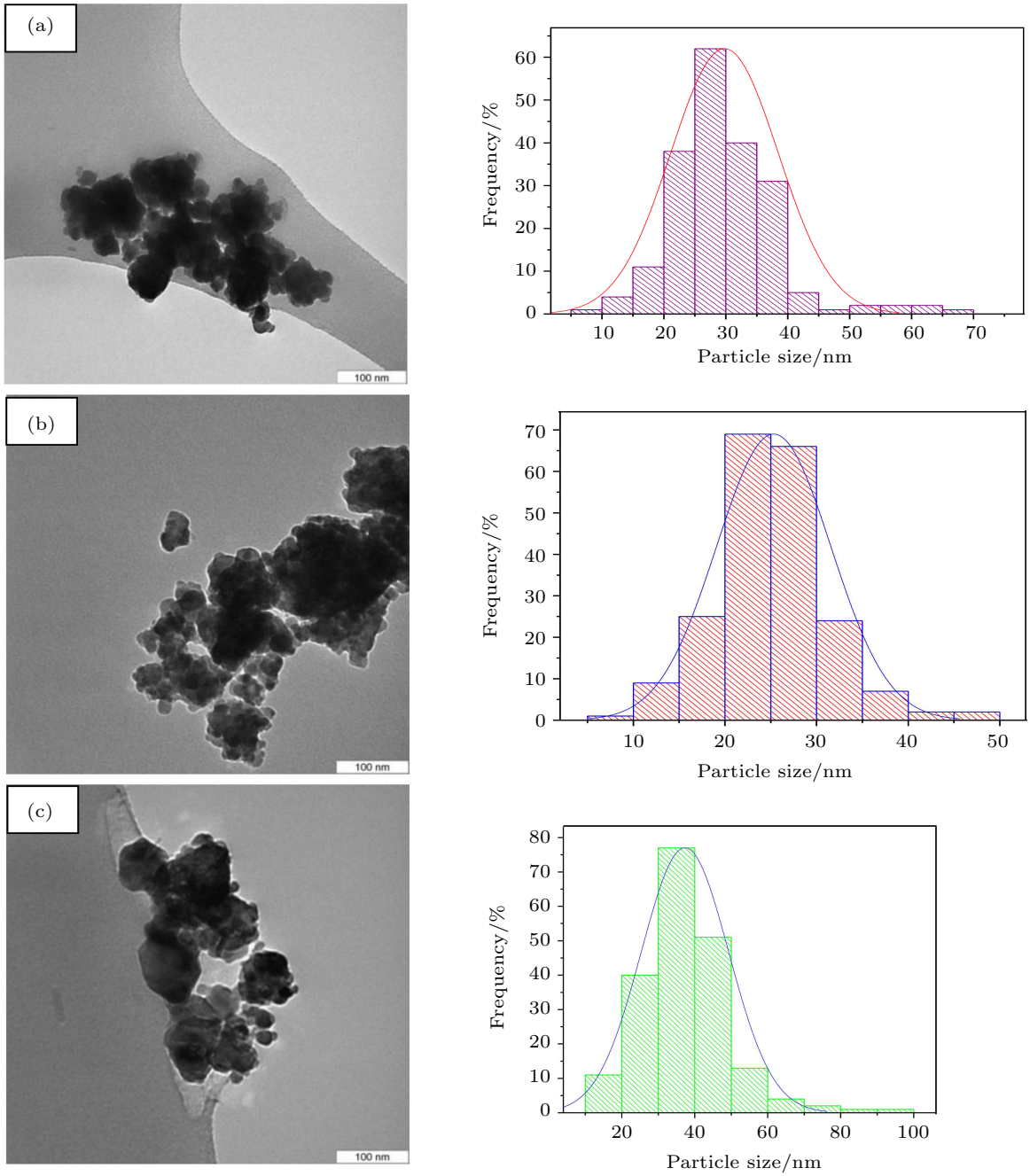


Fig. 7. (color online) TEM images accompanied with their particle size distribution histograms of the 30-h-milling samples under (a) air, (b) argon, and (c) oxygen atmospheres after annealing at 600 °C.

The XRD patterns reveal that the single phase of Ni–Zn ferrite is formed in each of all the samples after having been heated at 600 °C. In fact, the high-energy ball milling induces a large amount of energy to transfer from a grinding medium of the mill to the powder particles by frequently fracturing and cold welding. This action gives rise to obtaining a smaller crystallite size and higher surface area. Consequently, it remarkably increases the reactivity among reactants and significantly reduces the synthesis temperature and vaporization temperature compared with those samples prepared by the solid-state method.[5,17]

The XRD results indicate that the annealing of the 30-h-milling sample at 600 °C leads to two main variations in sample structure, i.e., increasing crystallite size and reducing lattice strain. It is determined that the average crystallite sizes increase to 18, 17, and 19 nm while the lattice strains decrease to 0.615%, 0.588%, and 0.558%, respectively in the 30-h-milling samples under air, argon, and oxygen atmospheres annealed at 600 °C.

The TEM images of the 30-h-milling samples in different atmospheres and annealed at 600 °C with their corresponding particle size distribution histograms are shown in Fig. 7 to better display the effects of milling atmospheres and annealing temperature. However, the particle growth takes place in each

of all the milled samples by the heating process, they present different distributions of particle sizes. By closely looking, the milled samples under argon atmosphere exhibit smaller particle sizes than those under the two other atmospheres after annealing at the same condition as confirmed by the XRD spectra. It is determined that the particle sizes are distributed in a range of about 12 nm–46 nm with an average size of 25 nm in the milled samples in the argon atmosphere while they are distributed in ranges of about 7 nm–70 nm and 15 nm–96 nm, with average sizes of 29 nm and 37 nm, respectively, in the milled samples in air and oxygen atmospheres.

3.5. Magnetic property characterization

With the particle size decreasing to a few nanometers, which is equivalent to increasing the surface-to-volume ratio, a crystallite lattice also extends only over a few nanometers. Consequently, the uncompensated magnetic spins attributed to the surface atoms become more important and may cause a net magnetization.[18–20] Therefore, for nonostructured Ni–Zn ferrite samples obtained from the different milling atmospheres, the magnetic properties are expected to depend strongly on the average particle size.

Room temperature M–H and B–H hysteresis loops for the 30-h-milling samples in different atmospheres are shown in Figs. 8(a) and 8(b), respectively. As seen from Fig. 8(a), the M–H hysteresis loops of the milled samples in argon, air, and oxygen atmospheres, with average particle sizes of 13, 15, and 16 nm, respectively, are shaped like an "S" with very small coercivity (H_c) values of about 89.2, 87, and 53.5 Oe (1 Oe = 79.5775 A·m^{-1}), respectively. According to Refs. [18] and [20], these are the characteristics of superparamagnetic materials. The Langevin equation is applied to nonlinear least fitting of the initial magnetization curves of the milled samples, and is expressed as

$$M(H) = M_s \left[\coth\left(\frac{\mu H}{K_B T}\right) - \frac{K_B T}{\mu H} \right], \tag{6}$$

where M_s, $M(H)$, T, K_B, and μ denote the saturation magnetization, the magnetization for an applied field H, the absolute temperature, the Boltzmann's constant, and the uncompensated magnetic moment, respectively.[21] The M_s value for the 30-h-milling samples in argon, air, and oxygen are estimated to be about 5.33, 4.53, and 3.44 emu/g, respectively, and their corresponding uncompensated magnetic moments are obtained to be about 0.192 μ_B, 0.164 μ_B, and 0.116 μ_B, where μ_B is the Bohr magneton. The variation of μ with average particle size indicates the effects of milling atmosphere on the milled samples microstructure and the cation distribution.

The lower values of saturation magnetization (M_s) in the milled samples can be related to the surface distortion of the small particle size because of the interaction of transition metal ions with oxygen atoms, which results in the reduced net magnetic moment in the particles. This is more obvious in ultrafine particles because of their larger surface-area-to-volume ratios.[22] A comparison of the M_s values reveals that the sample milled under argon has the highest M_s value whereas those milled under oxygen have the lowest ones. This may be due to the fact that the extra oxygen in the vial leads to the formation of non-stoichiometric products.

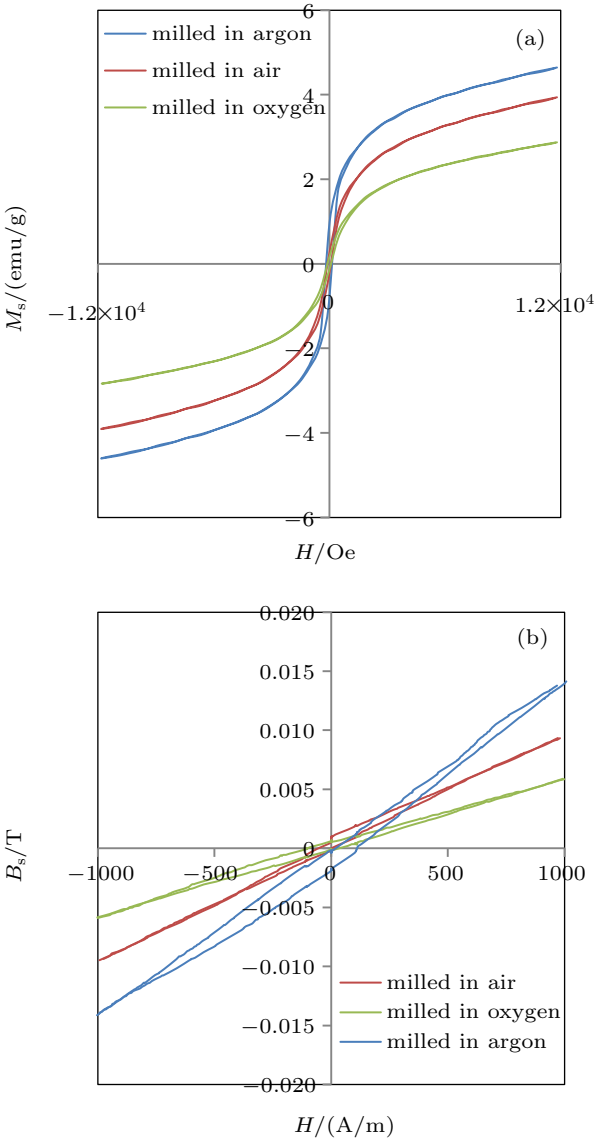


Fig. 8. (color online) Room temperature (a) M–H and (b) B–H hysteresis loops for 30-h-milling powders in different atmospheres.

From the B–H curves, different magnetization curves in the milled samples in different atmospheres as compared with the M–H curves derive from the interactions between the particles in a dense compact sample where the magnetization in an applied field is not simply the sum of the magnetization of isolated particles in that field. Furthermore, during compacting the milled powders the particle sizes, shapes, strains, and imperfections are all affected by the applied force which gives rise to different magnetization curves. The B–H curves also

indicate a lower value of saturation induction (B_s) for each of the three types of samples but with a higher value in argon about 0.02 T in an applied field of 1000 A/m. This also reveals the dependence of magnetic behavior on microstructural characteristics especially particle size, which arises from the different milling atmospheres. The linear-looking curve with lower H_c reveals the paramagnetic behavior of the sample with probably some superparamagetisms. Furthermore, it also suggests a very low amount of ordered magnetism in each of the 30-h-milling samples.

The values of volume fraction of the interfacial region (V_{if}) as a function of average particle size (d) in the milled samples in different atmospheres are estimated by using

$$V_{if} = 1 - \left[\frac{d-t}{t}\right]^3, \tag{7}$$

where $t/2$ is the thickness of the interfacial region, assumed to be about 0.5 nm.[18] The values of V_{if} are determined to be about 21%, 19%, and 18% in the milled samples under argon, air, and oxygen atmospheres, respectively. This indicates that the volume fraction of the total interfacial region is maximum for the sample milled in argon with the smallest average particle size of 13 nm and it reduces as the particle size increases in the milled sample in oxygen. The interfacial volume fraction is about 21% for the sample milled in argon, which is about 1.10–1.16 times larger than those for samples milled in air and oxygen. This accounts for the more or less similar magnetic response of the samples.

The M–H and B–H hysteresis loops of those 30-h-milling samples in argon, air, and oxygen, which are annealed at 600 °C for 2 h, are shown in Figs. 9(a) and 9(b), respectively. The M_s values increase to ∼35 emu/g, 28 emu/g, and 25 emu/g in the milled samples under argon, air, and oxygen after having been annealed at 600 °C, respectively, while their corresponding H_c values decrease to 26.77, 22.74, and 20.9 Oe in the M–H curves. These derive mainly from the heating process, which can significantly lead to the particle growth and reduce the lattice strain. Consequently, an order-cation distribution is obtained. From the B–H curves, it can also be observed that the magnetization is remarkably increased by heating the milled samples, which suggests that the number of particles with ferromagnetism is increased, thereby contributing to the ordered magnetism in the sample. The developing crystallinity of the annealed sample reveals a single spinel phase, which suggests that there is a combination of superparamagnetism (from small particles), paramagnetism (from the amorphous phase), and ferromagnetism. However, due to the lower coercivity and smaller particle size, the superparamagnetism is still dominant over the two other magnetic behaviors for all the milled-annealed samples at 600 °C.

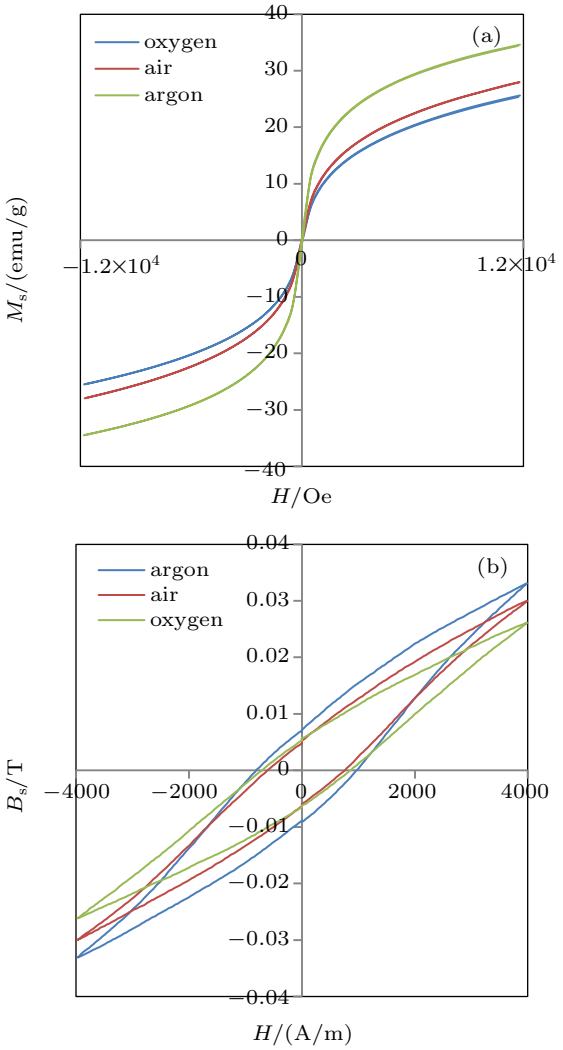


Fig. 9. (color online) Room temperature (a) M–H and (b) B–H hysteresis loops for 30-h-milling powders in different atmospheres, which are annealed at 600 °C.

4. Conclusions

The mechanochemical behavior of Zn/NiO/Fe_2O_3 powder mixture is investigated during high energy ball milling. It is found that the structure and phase formation are influenced not only by the milling time but also by the milling atmosphere. The increasing of the milling time from 0 to 30 h leads to the broadening of Bragg's peak widths as a consequence of the microstrain induced in powder particles, and the decreasing of crystallite size. The smallest crystallite sizes are achieved in the samples milled under argon while the largest sizes are obtained in those smaples milled under oxygen. The smallest crystallite size obtained under argon might be associated with either the formation of stoichiometric products or the conversion of Fe_2O_3 and Fe_3O_4 into each other during milling. The heat released from this conversion can also provide enough energy to produce a single phase Ni–Zn ferrite in the milling process. The VSM results indicate lower saturation magnetizations, which suggests the superparamagnetic behavior of the sample milled for 30 h, but higher M_s values

for samples milled under argon than those under the other two atmospheres. The annealing of the milled samples at a lower temperature of 600 °C not only keeps the desirable properties of nano-sized ball-milled Ni–Zn ferrite but also improves the magnetic properties.

References

[1] Shinde T J, Gadkari A B and Vasambekar P N 2008 *Mater. Chem. Phys.* **111** 87

[2] Atif M, Nadeem M, Grössinger R and Turtelli R S 2011 *J. Alloys Compd.* **509** 5720

[3] Raghavender A T, Biliškov N and Skoko Ž 2011 *Mater. Lett.* **65** 677

[4] Jahanbin T, Hashim M and Amin Mantori K 2010 *J. Magn. Magn. Mater.* **322** 2684

[5] Suryanarayana C 2001 *Prog. Mater. Sci.* **46** 1

[6] Hajalilou A, Hashim M, Nahavandi M and Ismail I 2014 *Adv. Powder Technol.* **25** 423

[7] Hajalilou A, Hashim M, Ebrahimi-Kahrizsangi R and Sarami N 2014 *Ceram. Int.* **40** 5881

[8] Hajalilou A, Hashim M, Ebrahimi-Kahrizsangi R, Mohamed Kamari H and Kanagesan S 2014 *Mater. Sci. Poland* **32** 281

[9] Yu L, Zhang J, Liu Y, Jing C and Cao S 2005 *J. Magn. Magn. Mater.* **288** 54

[10] Ismail I, Hashim M, Amin Matori K, Alias R and Hassan J 2011 *J. Magn. Magn. Mater.* **323** 1470

[11] Jalaly M, Enayati M H, Karimzadeh F and Kameli P 2009 *Powder Technol.* **193** 150

[12] Bid S and Pradhan S K 2003 *Mater. Chem. Phys.* **82** 27

[13] Smit J and Wijn H P J 1959 *Ferrites* (Philips Technical Library, Eindhovan, Netherlands)

[14] Vasoya N H, Vanpariya L H, Sakariya P N, Timbadiya M D, Pathak T K, Lakhani V K and Modi K B 2010 *Ceram. Int.* **36** 947

[15] Williamson G K and Hall W H 1953 *Acta Metall.* **1** 22

[16] Kingery W, Bowen H and Uhlmann D 2014 *Introduction to Ceramics*, 2nd edn. (New York: John Wiley & Sons)

[17] Kang Suk-Joong L 2004 *Sintering: Densification, Grain Growth and Microstructure* (Burlington, MA: Elsevier, Butterworth-Heinemann) pp. 27, 280, ISBN-10: 0750663855, ISBN-13: 978-0750663854

[18] Abdul Khadar M, Biju V and Inoue A 2003 *Mater. Res. Bull.* **38** 1341

[19] Richardson J T and Milligan W O 1956 *Phys. Rev.* **102** 1289

[20] Schuele W J and Deetscreek V D 1962 *J. Appl. Phys. Suppl.* **33** 1136

[21] Jiles D 1991 *Introduction to Magnetism and Magnetic Materials* (London: Chapman and Hall) p. 182

[22] Gharagozlou M 2010 *J. Alloys Compd.* **495** 217